The 9th of International Symposium on Transport Phenomena and Dynamics of Rotating Machinery
Honolulu, Hawaii, February 10-14, 2002

FLOW CHARACTERISTICS IN 2-LEG RIBBED INTERNAL COOLANT PASSAGES OF GAS TURBINE AIRFOILS WITH TURNING VANE AND FILM COOLING HOLE EJECTION

D. Chanteloup / denis.chanteloup@epfl.ch / EPFL – LTT – 1015 Lausanne – Switzerland
A. Bölcs / albin.boelcs@epfl.ch / EPFL – LTT – 1015 Lausanne – Switzerland

ABSTRACT

A study of flow, in three stationary models of two-pass internal coolant passages is presented, which focuses on the flow characteristics in the 180-deg bend region and downstream of the bend, where the flow is redeveloping. A stereoscopic digital Particle Image Velocimetry (PIV) system, measured all three velocity-components simultaneously to obtain mean-velocity and turbulence quantities of the flow field. The coolant passage models consisted of two square passages, each having a 20 hydraulic diameter length, separated by a web of 0.2 passage widths, and connected by a sharp 180 deg bend with a rectangular outer wall. Ribs were mounted on the bottom and top walls of both legs, with a staggered arrangement and at 45 deg to the flow. The rib height and spacing were 0.1 and 1.0 passage heights, respectively. They were equipped with extraction holes, to simulate holes for film cooling. Two series of holes were placed solely in the bottom wall, 4 holes were located in the bend, and 12 in the downstream leg. One of the configurations was also provided with a turning vane in the bend, and was equipped with a 60deg rib arrangement in the downstream leg. The measurements were obtained for a flow condition with a Reynolds number of 50,000. The global extraction through the holes was set to 50% of the inlet massflow. This paper presents new measurements, and a comparison of the flow between the two configurations, in the straight legs of the passages, in the bend regions, and details of the flow recovery from the bend in the second legs.

INTRODUCTION

For the design of gas turbine blades, a detailed knowledge of the physical phenomena in the passage is necessary. Although CFD simulations can provide a better understanding of these phenomena, the numerical heat transfer predictions are not yet sufficiently accurate for design purposes. To improve the performance of the CFD codes, a validation of the predictions is necessary, and detailed measurements of the flow structure in the passages are required for comparison, as noticed in [1].

[2] measured local heat transfer coefficients around the entrance to a normal hole. They reported considerable heat transfer coefficient variations (six times the plain duct local value) around the entrance. [3] noted that in presence of normal ribs, the heat transfer in the vicinity of the holes was increased by about 25%. The introduction, the location and the orientation of a turning vane in smooth 2-pass coolant channels, has been investigated in [4]. It was shown that turning vanes reduce the pressure losses and enhance the flow characteristics. [5] and [6], respectively predicted and measured, flow fields, pressure drop and heat transfer in 2-pass coolant passages with and without turning vanes. They showed that the turning vane decreased the pressure drop and homogenised the heat transfer distribution in the bend. Although detailed heat transfer measurements in coolant channels with film cooling holes are available in literature, to the authors knowledge the flow in such ducts has not been described; this is one objective of the present paper.

In the present study, the particle-image-velocimetry (PIV) method was employed for the investigation of the flow field in models of a stationary two-pass coolant passage. The measurement error introduced in high 3D flows, can be avoided by using a stereoscopic PIV setup ([7], [8]). A stereoscopic digital PIV system, based on the angular displacement method, was used for the present investigation ([9]). This PIV system measures all three instantaneous velocity components. Subsequently, an ensemble average of the velocity data, in identical spatial windows, is calculated to determine the mean and fluctuating velocity field.

This paper presents initial results from the Brite-Euram project, for Internal Cooling of Turbine Blades (ICTB [1]) measured with a PIV system. The objectives of [10] and [11] were to present results in a baseline configuration, and to determine the influence of the coolant extraction through simulating film-cooling holes, on the flow in the bend region. The specific objectives of the present paper are to determine the influence, of a turning vane introduction in the bend, and of the rib arrangement orientation in the downstream leg.

NOMENCLATURE

X	Cartesian coordinate in axial duct direction
Y	Cartesian coordinate in cross duct direction
Z	Cartesian coordinate in horizontal duct direction
θ	Cylindrical coordinate in streamwise direction
r	Cylindrical coordinate in radial direction
U	Mean velocity component in x direction
V	Mean velocity component in y direction
W	Mean velocity component in z direction
U_θ	Mean velocity component in streamwise direction in bend
U_b	Bulk mean-velocity
L	Test section length
D	Height and width of passage legs, D=100 mm
D_h	Hydraulic diameter D_h=D
B	Thickness of divider plate
P	Rib pitch
e	Rib height
S	Section length in bend at 90° section

EXPERIMENTAL SETUP

Test Facility

A sketch of the test section is shown in Figure 1. Air was the working medium, and was supplied by a continuously running compressor. The air enters the settling chamber with an inner diameter of 600mm, via a 150mm tube, and a conical entrance section with an angle of 30 deg. The settling chamber is equipped with a combination of perforated plates, honeycombs and meshes, to reduce unsteadiness and swirl in the flow.

Both studied configurations have the same inner geometry characteristics. The first (called *No Vane*) configuration test section is a two-pass, cooling passage model, of a gas turbine blade. The flow path in the downstream and upstream passages has a cross-section of $100\times100mm^2$, with a corresponding hydraulic diameter, $D_H = 100mm$, and a length of $20D_H$. The outer walls of the test section are made of 5mm thick extruded Plexiglas to obtain good optical properties for the PIV experiment. In the straight-corner 180 deg bend, the clearance between the tip of the divider plate and the outer wall is equal to 1 D_h. The thickness of the divider plate, or web, between the two passages is $0.2D_H$. The tip of the divider plate is cylindrically shaped with a $0.1D_H$ radius. Square ribs with an angle of 45 deg to the passage centreline, rib heights of 0.1 hydraulic diameters ($e/D_H = 0.1$), and rib spacing of 10 rib heights ($P/e = 10$) are mounted in a staggered arrangement on the top and bottom wall of the passage. The ribs in the bend region and the dimensions of the bend are shown in Figure 1. Eighteen ribs are mounted on each of the top and bottom walls, in each of the upstream and downstream passages of the model (18*4). The second configuration also called the *Vane* configuration, has the same inner geometry characteristics, except that the ribs downstream of the bend are oriented with an angle of 60deg to the passage centreline (see Figure 2). The *Vane* configuration is also equipped with a semi-circular turning vane placed into the bend. The $0.1D_H$ thick turning vane has a mean radius of $0.6D_H$, and is provided with $0.1D_H$ diameter rounded tips. The tips extend up to X=0.05 into the straight upstream and downstream legs. Both configurations have two series of holes for film cooling simulation. It has been chosen to place these holes solely in the bottom wall. The total mass flow through the holes is 50% of the mass flow in the test model. The first series of holes is placed in the bend region, $0.2D_H$ apart from the end wall. 4 $0.073D_H$-diameter holes are equally displaced between the leading, and the trailing outer walls. Twelve $0.082D_H$-diameter holes are located downstream of the bend, the rib pitch to hole pitch ratio is set to 2, in order to have two holes per rib-pitch, leading to a hole pitch to hole diameter ratio of 6. This series is situated on the bottom wall downstream leg centreline (Z=-0.6).

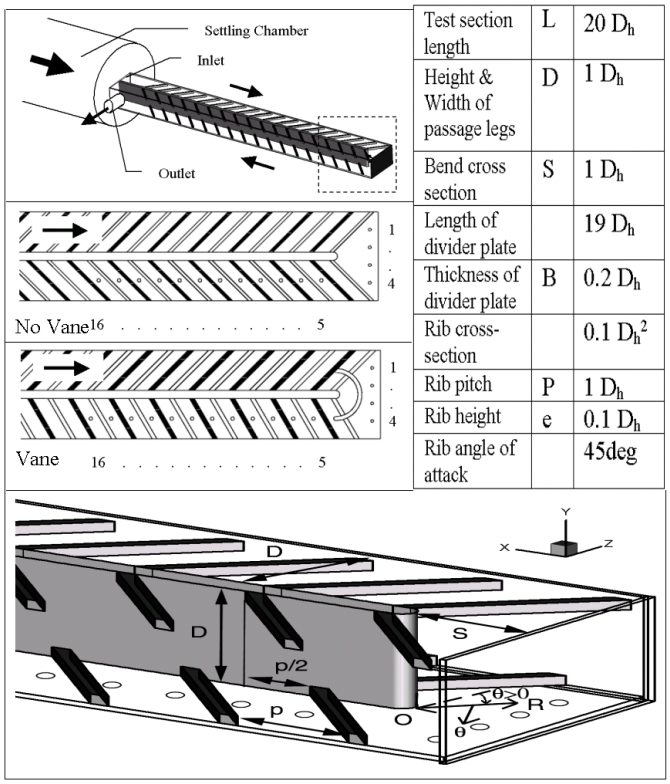

Test section length	L	20 D_h
Height & Width of passage legs	D	1 D_h
Bend cross section	S	1 D_h
Length of divider plate		19 D_h
Thickness of divider plate	B	0.2 D_h
Rib cross-section		0.1 D_h^2
Rib pitch	P	1 D_h
Rib height	e	0.1 D_h
Rib angle of attack		45deg

Figure 1 The internal coolant passage test facility and turn region details.

A modular concept was chosen for the test section that allows an easy exchange of the components. The test section, including the test section entrance, is turned 90 deg around the x-axis to obtain additional measurement planes, without changing the flow conditions in the passage. This allows an easy optical access to the positions of interest for the PIV measurements.

Measurement program and coordinate systems

The measurements were obtained with air as working medium, at a flow Reynolds number of 50,000 (corresponding to a bulk velocity: $Ub = 7.58m/s$), at the entrance of the test section. The Reynolds number is based on the 0.1 m hydraulic diameter with an air temperature of 20 C. Upstream of the test-rig, the mass flow is measured by means of a 5864S Brooks flow meter with a 1-percent accuracy. The turbulence level is approximately 3 percent at the model inlet. An experimental study was conducted to assess the effect a varying test section orientation on the flow. The small variations between the flow conditions are within the measurement uncertainty and can therefore be neglected for the experiments.

Extraction through the holes is adjusted by increasing the inner configuration pressure level. A butterfly valve, placed far downstream of the test section exit, adjusts the backpressure. A second 5864S Brooks flow meter, measures the exit massflow downstream of the butterfly valve, allowing to adjust a 50% Q_{in} extraction. Extractions through each hole have been characterised by hole velocity measurements. The velocity was measured at the outlet of the holes, with a 9mm diameter turbine flow meter probe placed 2mm apart from the hole (Y direction). The measured velocity is consequently an average of the free jet velocity profile. A precise positioning device allowed to place the probe at each hole outlet. The total massflow extracted, based on the hole velocity measurements, was found to be 48.5% of Q_{in}, yielding a 3% error in the hole massflow measurements.

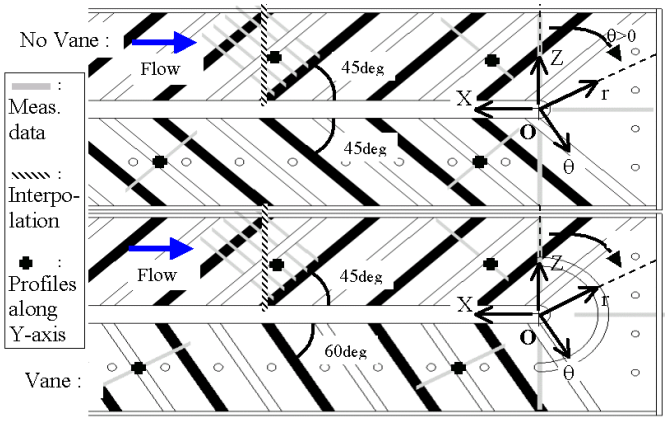

Figure 2: Measurement sections. The symbols represent the measurement lines (Y direction) that will be analysed in the next sections (Figure 7 and Figure 5).

Detailed measurements of the flow structure in the passage have been obtained in the bend, upstream ($3D_H$) and downstream ($4D_H$) of the 180 deg bend. The definition of the coordinate systems in the test facility is shown in Figure 2. A Cartesian coordinate system is used for the straight passages and a cylindrical coordinate system is used for the bend region. The origin for both coordinate systems is set on the bottom wall at the centre of the rounded end of the divider plate for both coordinate systems. In the Cartesian (*X, Y, Z)* system, *X* is defined as positive in the streamwise direction of the flow downstream of the bend exit, *Y* is defined positive vertically upwards in the horizontal test section orientation, and *Z* is defined as shown. In the cylindrical (θ, *r, Y*) coordinate system, the radial component r is defined as positive in the direction towards the outer wall, the streamwise component θ is defined as positive following the flow along the circular path centred on the centre of the circular bend tip, and *Y* is defined as for the Cartesian system.

PIV system

Di-Ethyl-Exyl-Sebacat (DEHS) from TOPAS is used as light scattering droplets for the PIV experiments. This light scattering liquid appeared non-toxic, compared to olive oil or paraffin oil used in the past. A DLR- made Aerosol Generator using Laskin Nozzles generates 1-3 µm-diameter DEHS droplets. The droplets are injected upstream of the settling chamber to guarantee a homogeneous seeding density in the test section. The particles produce good light scattering in the 90° direction according to the Mie law.

A 1.5-mm thick light sheet that illuminates the particles is created by a Quantel Twins B Nd-Yag double oscillator pulsed laser. The laser provides light pulses having a maximum energy of 320mJ at a wavelength of 532 nm. The time delay between a pair of pulses can be adjusted from 1µs to 1s with pulse duration of 5 ns. A plano-concave lens (-30 mm focal length) combined with two plano-cylindrical lenses (76.2 and 300 mm focal length) transform the beam into the vertical light sheet.

The imaging system consists of two independent Kodak ES1.0 cameras, each having its own PC. A Nikon Nikkor 55mm lens is mounted on each camera. The ES1.0 has a CCD interline transfer sensor with a pixel array of 1008(H) by 1018(V) pixels. Each pixel measures nine microns square with a 60 percent fill factor using a micro lens. The camera outputs 8 bit digital images with 256 grey levels. For a typical recording situation, the cameras are placed with an oblique angle of 4.3º at a distance of 0.7m from the light sheet plane. The pulse separation time is about 40 µs. The complete system, including laser, light sheet optics and camera, is mounted on a traversing system that allows an easy traverse to the position of interest.

The laser components (flash lamp and Q-switch) and the cameras are triggered by 10Hz TTL signals that are dispatched to all the elements with specific delays. As the different delays between both Flash lamps on the one hand, and between each Flash lamp and its Pockel cell on the other hand, are all different, they are generated by a programmable sequencer, the SEQUENCER Mod.919.4, made by the DLR Goettingen. The sequencer allows the generation of complex pulse patterns on multiple channels. The pulse width, the pulse interval, the number of pulses and the output channel number are freely programmable and their resolution is of 50ns.

The frame grabber is an Imaging Technology PCI frame grabber with 2 MB memory onboard. The PCs are equipped with 384 MB RAM and 14 GB hard disk space. During the PIV measurement series, 10 images are written in real time into the PC's RAM memory. Subsequently, the acquisition is stopped and the images are saved on the hard disk. The automation of the process allows storing a maximum of 5000 frames per measurement plane.

Data Reduction

The 3D PIV measurements are obtained from the combination of two 2-dimensional vector fields; each of them measured from two different observation locations (the right and left cameras). The recordings from the right and left cameras are interrogated independently with the PIV software package VISIFLOW from AEA Technology. The cross-correlation analysis method is used with an interrogation window size of 64 by 64 pixels and 50 percent overlap between the interrogation windows. The frames provided by the cameras have a 992*992-pixel^2 resolution, which yield a 30 by 30 velocity-vector field per measurement plane. The raw data contains a small number of spurious vectors (<0.1 percent). The vector field is filtered with a

predefined velocity magnitude threshold. Vectors that do not fall within the thresholds are removed and the remaining gaps are filled in with a weighted average of the surrounding vectors.

From the processed vector fields, the instantaneous three-dimensional velocity field can be reconstructed. Matlab homemade reconstruction software was developed at the EPFL-LTT. With angular PIV systems, where both cameras observe the light sheet from the same side, the corresponding interrogation positions in the right and left images do not match in general. Therefore, a calibration of the camera system is performed which also corrects for the distortion of the images in the lenses and the Plexiglas walls of the passage.

In addition to the mean-velocity field, the normal and shear stress quantities of the flow are required to evaluate numerical codes. In order to obtain PIV measurements in these forms, the statistical distribution of the velocity components is determined in identical spatial windows from a series of instantaneous PIV measurements. From these statistical distributions, the ensemble average and the statistical central moments are calculated to determine the desired mean-velocity field and Reynolds stresses.

Uncertainty analysis

[9], [12], [13] demonstrated the applicability of the presented stereoscopic PIV technique in detail. Following are comments on small variations from those measurements (see also [14]). For the present case, the mean number of particles per interrogation window (32 by 32 pixel^2) was set to 30. The average in-plane displacement of the particles is approximately 6 pixels, which is less than $0.25D_I$ in each direction, D_I being the characteristic dimension of the interrogation window. The optimal light sheet position for PIV measurement has the beam waist in the middle of the measurement section that provides a constant light sheet thickness in the measurement section. In the present investigation, the light sheet energy is so intense in the beam waist that the model Plexiglas walls are burned by the light sheet. The beam waist is placed outside of the section, which leads to a 10 percent variation of the light sheet thickness (mean thickness ≈ 1.2 mm) inside the section. An experimental study showed that the results are not significantly affected by the variation.

The estimation of the uncertainty of stereoscopic PIV velocity measurements requires the consideration of several aspects. Systematic errors occur due to the uncertainty in the determination of the geometrical parameter and the fabrication tolerances of the camera devices and lenses. Non-systematic errors are mainly due to the uncertainty in the determination of the average particle displacement in the interrogation region. The errors depend on the size of the interrogation region, the time separation between the laser pulses, the magnification of the recording, the out-of-plane velocity component, the turbulence of the flow, the length scale of the flow etc. The choice of the recording and interrogation parameters is therefore of significant importance for accurate and reliable velocity measurements. Using the method of [15], the mean value of the measured velocities is calculated by taking the instantaneous velocity measurements of the sample, summing the values, and dividing by the number of samples:

$$\bar{x} = \frac{1}{N}\sum_{i=1}^{N} x_i \qquad (1)$$

In the equations x is the *sample mean*. The number of observations N used to compute the estimates is called the *sample size*. Using the method of [15] The uncertainty for the mean velocity values of the present measurements is of order of 1 percent with a confidence level of 95 percent. The uncertainty of the mean velocity depends on the normal stresses and as a consequence is higher in regions where the turbulence level is high. Further details of the uncertainty method are given in [13].

RESULTS AND DISCUSSION

The objectives of the present paper are to determine the influence of a turning vane, combined with film-cooling flow extraction on the flow fields, upstream, inside and downstream of the bend region, and to provide new measurements of flow in internal 2-pass coolant channels for CFD validation. The following are data and discussion on these topics.

Extraction characteristics

The flow field in the tested channels is incompressible, and therefore pressure driven, yielding the pressure boundary conditions to play a major role in the flow characteristics. The pressure level (the static pressure compared to the atmospheric pressure at the channel inlet, $1D_H$ upstream of the 1st rib module) was set to 2456N/m^2 and 2571N/m^2 in the *No Vane*, and the *Vane* configurations respectively. The static pressure drop between the inlet and the outlet ($1D_H$ downstream of the last rib module) is 252N/m^2 in the baseline configuration, and 245N/m^2 in the "hole" configuration. This confirms the trend shown by [4], which observed a decrease of pressure drop, as a turning vane is introduced in a 180deg turn. The plenum chamber for the discharge of the hole flow is the laboratory room, and thus its pressure is the atmospheric pressure. Note that the rather high pressure-level in the test sections is due to the outlet butterfly valve adjusting the extraction to 50% Q_{in} for the entire channels. Tests have shown the pressure-level does not influence the static pressure distribution along the configuration.

Massflow measurements have been performed for each hole, quantifying the ejection distribution along the channels. Figure 3 gives details of the massflow distribution, as well as the bulk massflow present in the channel with regard to the hole number. Both quantities are normalized by the inlet massflow, 0.089kg/s. Note that upstream of the 1st hole, the bulk massflow ratio is 1, and 0.5 downstream of the 16th hole.

The mass flow extracted from the bend is 5% higher in the *Vane* configuration, than in the *No Vane*. The ejection through each hole of the bend is approximately constant, 2.3% of Q_{in} in the *No Vane*, and 2.5% of Q_{in} in the *Vane* configuration. This leads to a loss of the inlet massflow in the bend of 9.2% and 9.5% in the *No Vane* and *Vane* configurations, respectively.

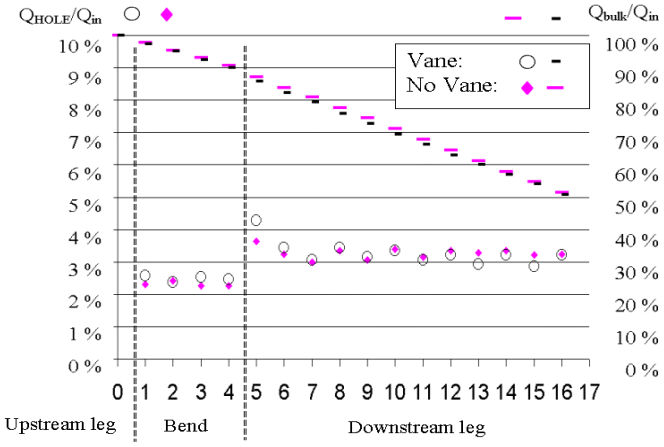

Figure 3: Hole velocity profile and remaining bulk massflow along both configuration centrelines.

As the flow is recovering the rib induced developed flow downstream of the bend, the ejection through the holes becomes constant in the *No Vane* channel, and remains fluctuating in the *Vane* channel. From the 2nd to the 6th rib module, 6.5% of Q_{in} is ejected per rib module. It decreases slightly in the *Vane* test section with 6% in the 5th and 6th rib modules. A periodicity of the ejection is noticeable between every first and second hole, in each rib module. The ejection through every second hole, of each rib module, is greater than through the first hole. Differences of 10% occur in the *Vane* configuration, and 10% to 2% from the 2nd to the 6th rib module in the *No Vane* case. The periodicity can be attributed to the recirculating zone downstream of each rib, where the static pressure is less than after the flow reattachment in front of the bottom ribs (in location of every 2nd hole). Although not illustrated here, it can be shown that the recirculating flow reattaches 2 rib heights downstream of a 45deg inclined rib, in a direction normal to the rib, (see [13]); this excludes the 1st hole location downstream of a rib. With a 60deg inclined rib, the reattachment length is 3 rib heights; this includes the 1st hole downstream of the rib. The difference in velocity profiles in the vicinity of the hole, more than the turning vane presence, is thought to be responsible for the differences between the *No Vane* (45deg), and the *Vane* (60deg) configurations. Note that the influence of the bend, and of the turning vane, can be noticed in the 1st rib module downstream of the bend, increasing the massflow through the 1st hole.

Flow in the bend region

The flow in the upstream leg developed region near a 180deg, in cooling channels, has already been described by [16] and [10]. It is strongly influenced by the ribs on both opposite walls, yielding, when no extraction occur, two counter rotating vortices, both occupying half of the cross section. [11] has described the extraction influence in the near upstream region of a 180deg bend. The flow is attracted towards the wall, with extraction yielding a non-symmetrical secondary flow. This type of flow, dominated by the extraction, occurs in both cases of the present study.

Figure 4 gives a flow comparison in both the *No Vane* and *Vane* configurations. Mean streamwise velocity contours and secondary flow vectors are presented. They were obtained two rib modules upstream, at θ=0, 90 and 180 deg in the bend and 10 rib modules downstream, where the flow recovers from both the bend, and extraction effects. These average velocity results were obtained from 1250, full-field data sets. For this set of results, the orientation of the view is always into the oncoming flow, with the web at the left-hand side of the figure.

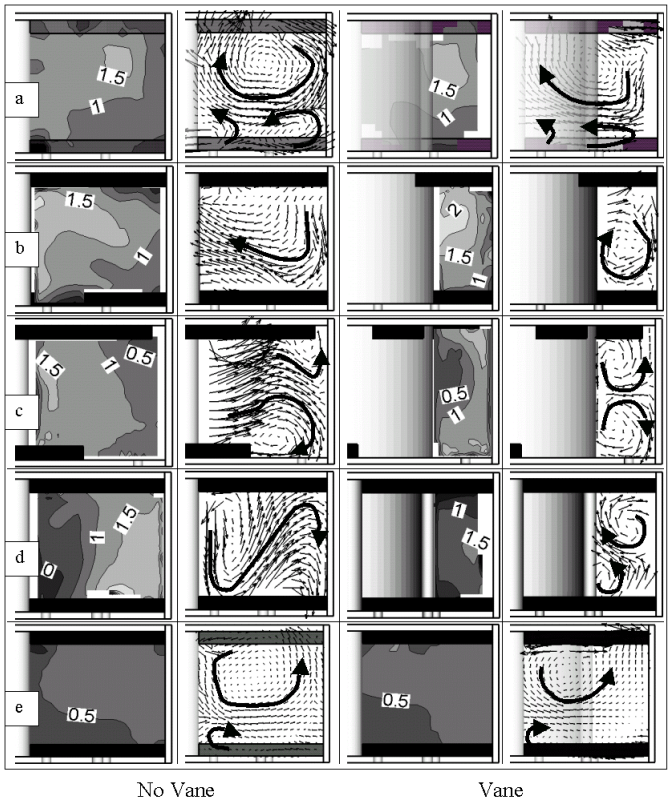

Figure 4: Mean streamwise velocity contours and secondary flow vectors obtained at: a:X=2nd-rib-upstream, b:θ=0°, c:θ=90°, d:θ=180°, e:X=10th-rib-downstream of the bend. The contour lines values, U_θ , are plotted on the figures (U_θ /Ub).

Two rib modules upstream of the bend, the flow fields in both *No Vane* and *Vane* configurations are very similar. Streamwise velocity regions have the same shape and, the vortex sizes and locations are the same. For further details, the reader is referred to [11]. From these results, it can be concluded that the influence of the guide vane is negligible on the upstream flow, compared to the influence of the extraction.

The flow in the bend region is more complex than in the ribbed region. The flow in the bend starts with the secondary structure from the ribs at θ=0deg. At θ=0deg, the streamwise velocity distribution and the secondary flow patterns in the centre region, show the effects of the bend (Figure 4). The streamwise flow near the inner web has begun to accelerate, and a high streamwise velocity core is present in the channel centre region. The outer part of this high streamwise core is attached to the turning vane outer wall. The streamwise component reaches peak values of $2U_b$, in the area $Y \geq 0.4$, instead of $1.5U_b$ in the *No Vane* case. This indicates that the guide vane presence, reducing the cross section surface, accelerates the flow field. A large vortex, present in the *No*

Vane configuration, is identifiable in the *Vane* secondary vector field. Note that no measurement is available in the region $r < 0.6$, due to a poor optical access.

At θ=90deg, the streamwise velocities of the flow have decreased near the web in the *Vane* case. Although not shown here, from θ=45deg toθ=90deg, the secondary flow field has been strongly modified in both configurations. The extraction has sucked the flow towards the bottom wall. In the *Vane* case, the ratio massflow affected by the extraction to extracted massflow is 20%, and 9.2% in the *No Vane* case, since in the *Vane* case, half of Q_{in} is directed in the r<0.6 region and not affected by the extraction. The *Vane* secondary flow is very symmetric compared to the *No Vane,* and to the *no-extraction* ones of [10]. The vane effect on the streamwise velocity field is also noticeable. A region of low streamwise velocity is detected near the guide vane, for $0.5 < Y < 0.8$, indicating a small recirculating cell in the adverse pressure gradient zone downstream of the θ=90deg cross section (110deg<θ<150deg). Note that the streamwise velocity maximums are less than at θ=0deg, indeed the extracted flow through the first two holes, has decreased the affected massflow of 5%Q_{in}. Considering these results, the heat transfer on the bend end wall is expected to be symmetric in the *Vane* channel.

At θ=180deg, a small region of recirculation occurs near the web, and the bottom wall in the *No Vane* duct. The streamwise velocity fields have been influenced in different ways by the 2 bends. In the *No Vane* duct, the centrifugal forces direct the flow with high streamwise velocity (>1.5U_b), towards the outer wall. A small recirculating zone is attached to the web tip. In the *Vane* case, the streamwise velocity magnitude near the outer wall is smaller (<1.5U_b); this is due to both the turning vane, and the massflow extracted through the bend. Further details on the streamwise velocity are given in Figure 6 and Figure 7. The secondary flows are very different in both configurations; the flow goes from the top to the bottom wall along the web, crosses the channel up to the top outer wall, and goes down to the bottom wall along the outer wall, in the *No Vane* duct. Two vortices occur in the *Vane* channel. Their rotation directions are the opposite from θ=90deg; they have changed between θ=90deg and θ=135deg.

Downstream of the extraction ($X > 6$), the secondary flows are redeveloping, having a similar shape to the secondary flow in the upstream leg. The velocity magnitudes are twice lower than in the upstream leg, due to the 50% Q_{in} extracted from the channel. The rib orientation in the downstream leg has distributed the flow, symmetrically compared to the inlet flow. The secondary flow field has also recovered from the bend, but is still influenced by the extraction. The symmetrical shape around the $Y = 0.5$-axis observed in the *no-extraction* channel of [10], is not recovered. Note that in the outer corner of the bottom wall, a small difference occurs between the *No Vane* and *Vane* cases; the secondary flow is at rest in the *Vane* case. This is attributed to the 60deg rib orientation instead of 45deg.

The conclusion from this data is that the addition of a turning vane in the bend region, strongly influences the flow in the bend, and near the downstream bend region. In both the upstream and far downstream legs, the turning vane does not affect the flow, and the heat transfer distributions are expected to be periodic and similar.

Flow in the downstream leg

Downstream of the bend is another region with relatively large variations in heat transfer. Figure 5 presents streamwise velocity contours of the downstream turn region, and gives further details of the flow characteristics in the streamwise direction. The region presented is located in the near downstream bend area, where extraction occurs ($0 < X < 4$). The centre part of the channel is plotted ($0.3 < Y < 0.7$).

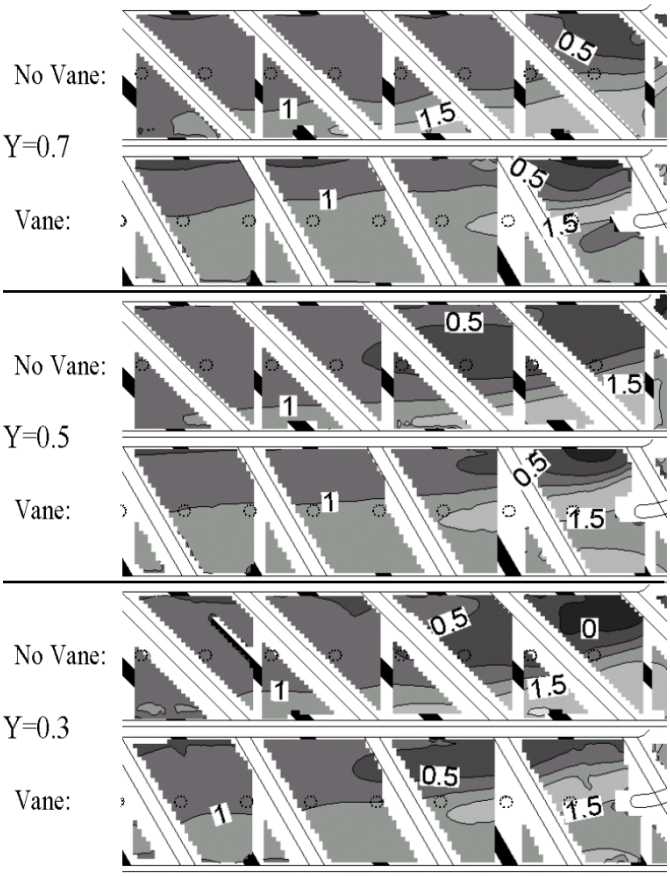

Figure 5: streamwise velocity contours immediately downstream of the bend, 0.0 < X < 4.0 at three distances from the bottom wall (U/Ub).

The turning vane has a great influence on the flow downstream of the bend. Differences between the *No Vane* and *Vane* configurations, appear in the streamwise velocity contours. In the *No Vane* channel, the streamwise velocity component recovers from the bend effect quite similarly to the case with no extraction (see [11]). The flow homogenises in the spanwise direction as X increases, the rib induced effects becoming preponderant. The high-speed region (U_θ/U_b>1) occupies the outer half part of the duct (Z<-0.6) and extends up to X>2. In the *Vane* case, the higher streamwise velocity region takes place around the centreline, ($U > 1.5$ in $-0.7 < Z < -0.4$). The fraction of massflow ($\approx 50\% Q_{in}$) directed at $\theta = 0\,\text{deg}$, between the web and the turning vane, undergoes the curvature effects. The streamwise profile in this region ($Z > -0.6$), is similar to the one in a

case without extraction (see [10]). Near the vane outer wall, the velocity is lower, since 9.94% of Q_{in} was extracted through the bend holes. Although not shown here, a high shear stress can be observed in the mixing layer, between the inner and outer flows.

Near the web, a recirculating zone appears at the web tip for Y<0.5. The recirculating cell near the web has almost disappeared, as a turning vane was introduced into the bend. This should be a great benefit to a smoother distribution of heat transfer coefficients in the near bend region ($0 < X < 1$).

Both streamwise velocity profiles recover from the bend in a very different manner. As the extraction influence mainly acts on the secondary flow field (see [11]), the turning vane influences the streamwise profile, leading to a streamwise velocity distribution, with small gradients at the bend exit.

Turning vane influence

A description of velocity components in the developed flow region of a similar coolant passage was presented by [17]. The measurements showed that the flow in a passage with 45deg rib arrangement, requires a longer development length than with 90deg rib arrangement; at least 8 rib modules are needed to achieve a developed flow condition for the mean velocity components, and 12 rib modules are required for the turbulent kinetic energy of the flow. In the present configurations, 18 rib-modules are placed in the upstream leg, to produce a developed flow field before the 180-deg bend. The analysis of the developed flow characteristics in a *no-extraction* configuration was presented in [10] Figure 3. For the obvious reason of space in this paper, the Figure 3 for the *No Vane* and *Vane* channels, is not plotted here. However the major results can be summarised as follow: The flow in the *no-extraction* configuration has shown to be developed in the upstream 16th rib module, and the periodicity going with this developed state is extending up to the bend inlet. Instead, in the *No Vane* and *Vane* configurations, the flows in the 16th rib module have already undergone the bend influence; the streamwise velocity variations reach 15% at the bend inlet location.

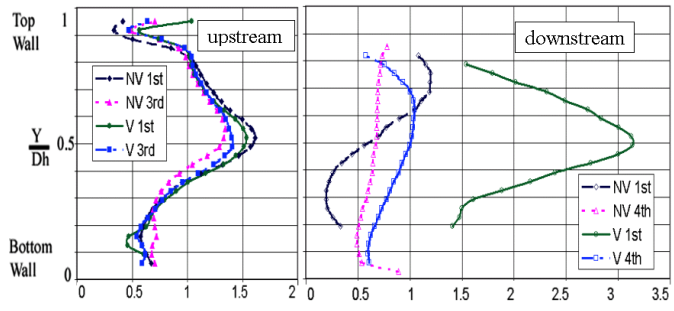

Figure 6: Centre line velocity profiles ratios (No-Vane/Baseline and Vane/Baseline) upstream and downstream of the bend. E.g. Figure 2 for exact locations in the rib modules.

Figure 6 verifies these observations. Velocity profile ratios are plotted along the configuration centreline (Z=0.6 upstream, Z=-0.6 downstream). They are describing the velocity evolution from the bottom to the top wall, i.e. along the Y-axis. Profile positions are described in Figure 2, they are located beyond the top rib of each rib module in the downstream leg, and between the top and the bottom rib in the upstream leg. Values greater than 1, indicate parts where velocity components in the present configurations are greater than in the *no-extraction* configuration, and vice versa.

The differences induced by the extraction are clearly noticeable on the Figure 6, left hand side graph, which represents upstream profiles. Between the 3rd and the 1st upstream ribs, the ratios have changed, whereas the reference *no-extraction* flow is the same (See [10]). This indicates that the extraction influences the flow far upstream of the bend. However, both *No Vane* and *Vane* cases are very similar, showing that the turning vane has only a minor impact on the flow in the upstream leg.

The profiles of Figure 6, right hand side, confirm the results plotted in Figure 5, downstream of the bend. The flow field is recovering from the bend effect. The secondary flow field rapidly becomes rib dominated. The streamwise velocity ratios are mainly lower than 1, indicating that the bulk velocity diminishes as the massflow extracted, increases. It can be noted, on the one hand, the great differences between the profiles of a same configuration, as X increases. This indicates that the flow is not periodic. On the other hand, at the same X location, the profiles are different from one configuration to the other, showing that the guide vane perturbs the bend downstream flow, especially in the regions where the velocity gradients are high, as here at $Z = -0.6$.

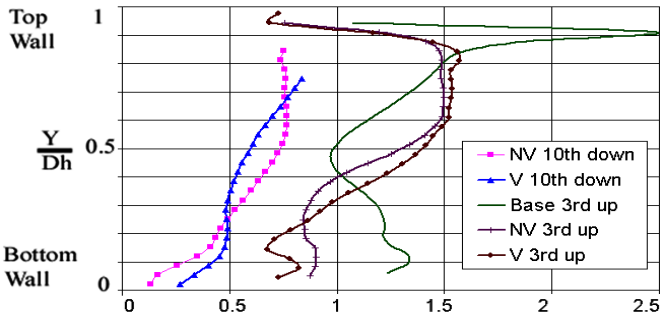

Figure 7: Comparison of the centre line velocity profiles upstream and downstream of the bend. E.g. Figure 2 for exact locations in the rib modules.

Figure 7 shows the *No Vane* and *Vane* streamwise profiles, 10 rib modules downstream of the bend. It compares the profiles to those of the same cases, in the fully developed upstream region (3 rib modules upstream of the bend). It also plots a reference profile of the fully developed flow in a configuration without extraction. The main conclusions driven from this graph, are that the flow has almost recovered from the bend effects, but not from the extraction. Indeed, the profiles 3 ribs upstream, and 10 ribs downstream are similar at a factor 2, this factor 2 is due to the mass flow lost through the holes (Q_{out}=Q_{in}/2). It indicates that 4 ribs downstream of the extraction end (end at $X = 6$), the flow has reached the upstream, fully developed profile. But, the flow hasn't recovered the fully developed shape of a case without extraction. The extraction influence extends far downstream of the region of extraction. Note that at $X = 10$, small differences occur between the *No Vane* and *Vane* streamwise velocity profiles. This is attributed to the different angle of

the ribs to the centreline (45deg instead of 60deg).

These results completed by [10] and [11] provide a set of measurements that can be used to evaluate codes, and turbulent transport models, in 2-pass ribbed channel. These flows in the "developed periodic" upstream leg, in the bend region, and in the downstream leg, reflect effects that will probably be obtained in most coolant channels, with and without extraction. As the flow is highly turbulent and pressure driven, the data provide a good test for codes to predict flow and heat transfer, with various turbulence models, wall approximations and meshing strategies.

CONCLUSIONS

Three-dimensional velocity measurements were obtained in a 2-pass blade coolant passage model. The model length, the rib angle, the rib locations and the geometry of the web between the coolant passage legs, were representative of gas turbine cooling designs. Here is presented a comparison between two similar configurations, provided with bleed holes, simulating the holes for external film cooling of blades. One configuration is also provided with a turning vane in the bend, and with a 60deg rib arrangement in the downstream leg.

Adding a turning vane, changing the rib orientation from 45deg to 60deg, and having a high ratio between the channel inlet mass flow, and the extracted mass flow, strongly influence the flow in the 2-pass cooling channel. The flow field is not significantly influenced upstream of the bend. In the bend, the turning vane strongly modifies both streamwise and secondary flow fields. In the near downstream region ($X \leq 4$), the flow is still perturbed by the turning vane presence. Downstream of the extraction ($X \geq 6$), the streamwise and secondary flows have recovered from the bend and turning vane effects, but they are still dominated by the extraction, and the flows haven't recovered the *no-extraction* fully developed shape.

The turning vane modifies the flow extraction mainly in the bend, and in the first rib module downstream of the bend. Farther downstream, differences are due to the rib arrangement angle.

Measurements along the centre-line of the channel, show details in the streamwise velocity profile. The data presented in addition with that given in [10] and [11], can be used to evaluate numerical simulation methods, and meshing strategies, turbulence or wall treatment models. The unsteady character of the flow, may require time dependent numerical techniques to accurately simulate the flow. The area near the web, and probably upstream of the bend, is likely to have large variations in heat transfer, due to the high variations in streamwise velocity, and may produce hot and cold spots, and possibly increased stresses with their thermal gradients.

ACKNOWLEDGMENTS

This study was funded by the Swiss Office of Science in cooperation with the BriteEuram Internal Cooling of Turbine Blades project (contract number: BRPR-CT97-0600, project number: BE97-4022).

REFERENCES

1. Rowbury, D., Parneix, S., Chanteloup, D. and Lees, A. (2001). *Research into the influence of Rotation on the Internal Cooling Turbine Blades*. Proceedings of the AVT Symposium - Heat transfer and cooling in propulsion and power systems. Loen, Norway. 2001.
2. Byerley, A.R., Jones, T.V. and Ireland, P.T. (1992). *Internal cooling passage heat transfer near the entrance to a film cooling hole: Experimental and computational results*. Proceedings of the International Gas Turbine & Aeroengine Congress & Exhibition. Cologne, Germany. 1992. 92-GT-241.
3. Shen, J.R., Wang, Z., Ireland, P.T. and Jones, T.V. (1996). *Heat transfer enhancement within a turbine blade cooling passage using ribs and combinations of ribs with film cooling holes.* Journal of Turbomachinery, 118 July 1996, 428-434.
4. Plevich (1984). *Pressure losses and flow visualisation in rectangular duct 180deg turns* (Arizona State University), MS Thesis.
5. Bonhoff, B., Leusch, J. and Johnson, B.V. (1999). *Predictions of flow and heat transfer in sharp 180-deg turns of gas turbine coolant channels with and without turning vanes*. Proceedings of the 33rd National Heat Transfer Conference. Albuquerque, New Mexico, USA. 1999. NHTC99-299.
6. Schnieder, M., Höcker, R. and von Wolfersdorf, J. (2001). *Heat transfert and pressure loss in a 180°-turn of a rectangular, rib roughened two passage channel*. Proceedings of the ExHFT-5: 5th world conference on experimental heat transfert, fluid mechanics and thermodynamics. Thessaloniki, Greece. 2001.
7. Prasad, A.K. and Adrian, R.J. (1993). *Stereoscopic Particle Image Velocimetry Applied to Liquid Flows.* Experiments in Fluids, 15 ,49-60.
8. Westerweel, J. and Nieuwstadt, F.T. (1991). *Performance Tests on 3-Dimensional Velocity Measurements with a Two-Camera Digital Particle-Image-Velocimeter*. In: *Laser Anemometry*), Vol. 1, 349-355.
9. Schabacker, J. and Bölcs, A. (1996). *Investigation of Turbulent Flow by means of the PIV Method*. Proceedings of the 13th Symposium on Measuring Techniques for Transonic and Supersonic Flows in Cascades and Turbomachines. Zurich, Switzerland. 1996.
10. Chanteloup, D. and Bölcs, A. (2001). *PIV investigation of the flow characteristics in 2-leg internal coolant passages of gas turbine airfoils*. Proceedings of the Euroturbo, European conference on turbomachinery fluid dynamics and thermodynamics. Firenze, Italy. 2001.
11. Chanteloup, D. and Bölcs, A. (2001). *PIV investigation of the flow characteristics in 2-leg internal coolant passages of gas turbine airfoils with film cooling hole ejection*. Proceedings of the International Symposium on Experimental and Computational Aerothermodynamics of Internal Flows. Gdansk, Poland. 2001.
12. Schabacker, J., Bölcs, A. and Johnson, B.V. (1998). *PIV investigation of the flow characteristics in an internal coolant passage with two ducts connected by a sharp 180° bend.* Proceedings of the International Gas Turbine & Aeroengine Congress & Exhibition. Stockholm, Sweden. 1998. 98-GT-544.
13. Schabacker, J. (1998). *PIV investigation of the flow characteristics in an internal coolant passages of gas turbine airfoils with two ducts connected by a sharp 180° bend*. In: *Thesis* (Ecole Polytechnique fédérale de Lausanne), Vol. n°1816.
14. Raffel, M., Willert, C.E. and Kompenhans, J. (1997). *Particle Image Velocimetry. A practicle guide* (Springer), ISBN 3-540-63683-8.
15. Bendat, J.S. and Piersol, A.G. (1986). *Random data*. In: *Random data* (John Wiley & Sons, Inc.).
16. Schabacker, J., Bölcs, A. and Johnson, B.V. (1999). *PIV investigation of the flow characteristics in an internal coolant passage with 45° rib arrangement*. Proceedings of the International Gas Turbine & Aeroengine Congress & Exhibition. Indianapolis, Indiana, USA. 1999. 99-GT-120.
17. Bonhoff, B., Schabacker, J., Parneix, S., Leusch, J., Johnson, B.V. and Bölcs, A. (1998). *Experimental and numerical study of developed flow and heat transfer in coolant channels with 45 and 90 degree ribs*. Proceedings of the Turbulent heat transfer II. Manchester, UK. 1998. 99-GT-123.